Journal of Biology

BioMed Central

Open Access

Research article

A functional genomic analysis of cell morphology using RNA interference

AA Kiger*, B Baum*†, S Jones‡, MR Jones§, A Coulson§, C Echeverri¶ and N Perrimon*

Addresses: *Department of Genetics, Harvard Medical School, Howard Hughes Medical Institute, Boston, MA 02115, USA. ‡Genome Sciences Centre, British Columbia Cancer Research Centre, Vancouver V5Z 4E6, Canada. §MRC Laboratory of Molecular Biology, Cambridge CB2 2QH, UK. ¶Cenix BioScience GmbH, D-01307 Dresden, Germany. Current address: †Ludwig Institute for Cancer Research, University College London W1W 7BS, UK.

Correspondence: Norbert Perrimon. E-mail: perrimon@rascal.med.harvard.edu

Published: 1 October 2003

Journal of Biology 2003, **2:**27

The electronic version of this article is the complete one and can be found online at http://jbiol.com/content/2/4/27

Received: 17 April 2003
Revised: 17 July 2003
Accepted: 12 August 2003

Abstract

Background: The diversity of metazoan cell shapes is influenced by the dynamic cytoskeletal network. With the advent of RNA-interference (RNAi) technology, it is now possible to screen systematically for genes controlling specific cell-biological processes, including those required to generate distinct morphologies.

Results: We adapted existing RNAi technology in *Drosophila* cell culture for use in high-throughput screens to enable a comprehensive genetic dissection of cell morphogenesis. To identify genes responsible for the characteristic shape of two morphologically distinct cell lines, we performed RNAi screens in each line with a set of double-stranded RNAs (dsRNAs) targeting 994 predicted cell shape regulators. Using automated fluorescence microscopy to visualize actin filaments, microtubules and DNA, we detected morphological phenotypes for 160 genes, one-third of which have not been previously characterized *in vivo*. Genes with similar phenotypes corresponded to known components of pathways controlling cytoskeletal organization and cell shape, leading us to propose similar functions for previously uncharacterized genes. Furthermore, we were able to uncover genes acting within a specific pathway using a co-RNAi screen to identify dsRNA suppressors of a cell shape change induced by *Pten* dsRNA.

Conclusions: Using RNAi, we identified genes that influence cytoskeletal organization and morphology in two distinct cell types. Some genes exhibited similar RNAi phenotypes in both cell types, while others appeared to have cell-type-specific functions, in part reflecting the different mechanisms used to generate a round or a flat cell morphology.

Background

The morphological diversity of animal cells results largely from differences in the lineage-specific expression and control of cytoskeletal regulators. Cells in culture have been widely used to characterize morphogenetic events, for example the dynamics and organization of filamentous actin and microtubules in adherent and motile cells. Few metazoan cell systems, however, permit the use of genetic analysis to identify the complement of genes contributing to the generation of cell shape.

RNA interference (RNAi) has revolutionized the functional analysis of genes identified by genomic sequencing [1-3]. Several factors make RNAi in *Drosophila* cell cultures an excellent approach for such functional genomic analysis of animal cell form. The availability of well-annotated *Drosophila* genomic sequence simplifies the design of gene-specific double-stranded RNAs (dsRNAs) [4]. Furthermore, the *Drosophila* genome encodes homologs of over 60% of human disease genes [5] and lacks some of the genetic redundancy observed in vertebrates. RNAi in *Drosophila* cells is efficient, reducing or eliminating target-gene expression to elicit partial to complete loss-of-function phenotypes upon the simple addition of dsRNA to the culture medium [6]. Finally, the well-established genetic techniques for *Drosophila* allow comparisons to be made between loss-of-function cell-culture phenotypes and those observed in tissues of corresponding mutant flies.

In order to develop a cell-based approach for the study of gene functions involved in morphogenesis, we developed a high-throughput RNAi screening methodology in *Drosophila* cell cultures that is applicable to the study of a wide range of cellular behaviors (Figure 1a). This approach involves the following steps: first, the design and synthesis of a gene-specific dsRNA library; second, incubation of *Drosophila* cells with the dsRNAs in 384-well assay plates (in serum-free medium or with transfection reagents, depending on the cell line); and third, optional induction of a cell behavior, followed by detection of luminescent or fluorescent signals using a plate reader or an automated microscope.

Here, we describe the establishment of an RNAi functional approach applied to the study of cell morphology. Using images acquired by automated microscopy, we visualized phenotypic changes resulting from reverse-functional analysis

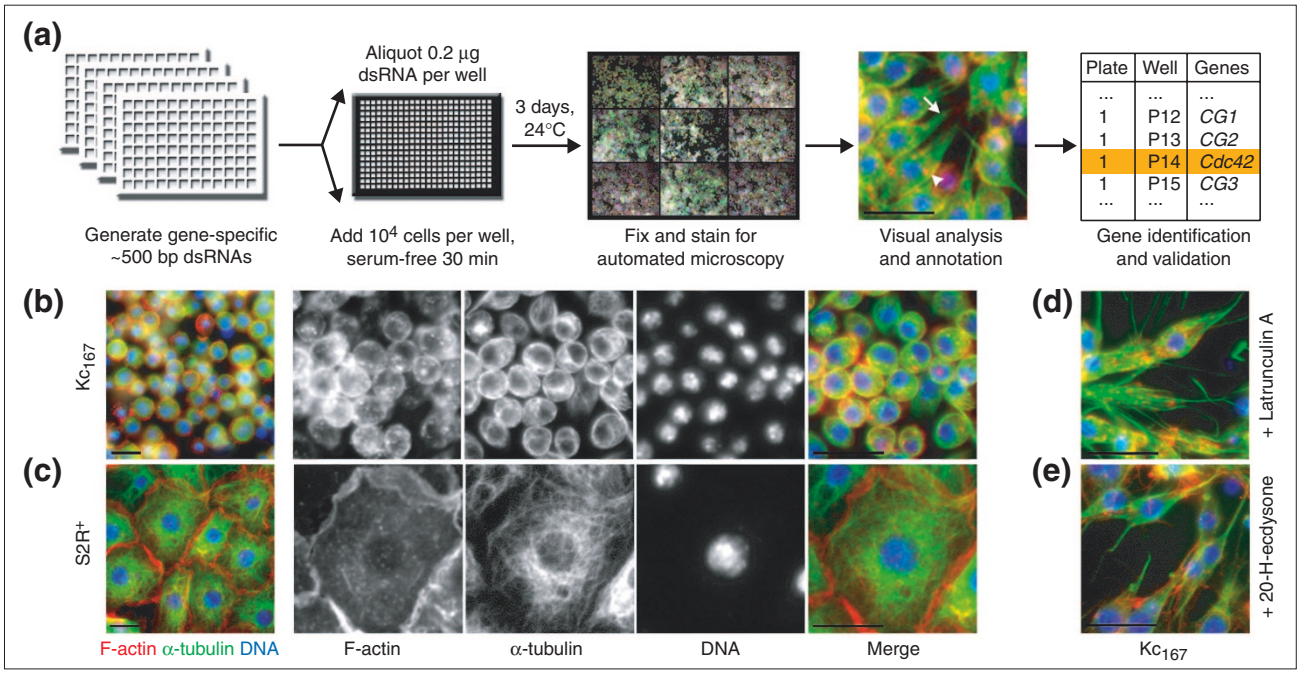

Figure 1
High-throughput RNAi screens by cell imaging. **(a)** Cellular phenotypes were visualized 3 days after the addition of dsRNA. In the example shown Kc_{167} cells changed shape from round to polarized, with F-actin puncta (arrowhead) and extended microtubules (arrow), in response to *Cdc42* dsRNA. **(b)** Kc_{167} and **(c)** $S2R^+$ cells at low (left) and high (far right) magnifications, fluorescently labeled for F-actin (red), α-tubulin (green) and DNA (blue). Cell-shape changes could be induced using drugs that affect the cytoskeleton or using extracellular signals, as seen upon treatment of Kc_{167} cells with **(d)** latrunculin A or **(e)** 20-hydroxyecdysone (20-H-ecdysone). Scale bar, 30 µm.

by the treatment of *Drosophila* cells in culture with gene-specific dsRNAs. We were able to observe and characterize a wide range of phenotypes affecting cytoskeletal organization and cell shape, and from these, to identify sets of genes required for distinct round versus flat cell morphologies.

Results and discussion

Drosophila cell morphology in cultures

We began by surveying existing *Drosophila* cell lines to identify those with distinct but uniform cell shape, size and adhesion properties. For a comparative study, we chose to further characterize two well-established lines, Kc_{167} and $S2R^+$ cells [7-9], because of their differences in cell shape. Although both lines apparently derived from embryonic hemocytes (blood cells), Kc_{167} cells are small and round (10 μm; Figure 1b), whereas $S2R^+$ cells are large, flat and strongly adherent to glass, plastic and extracellular matrix (averaging 50 μm; Figure 1c). The stereotypical morphology of each cell line could be modified in specific ways using drugs that perturb cytoskeletal function (for example cytochalasin, latrunculin, nocodazole or colchicine; see Figure 1d), ecdysone hormone treatment (Figure 1e), substrate-induced cell polarization (phagocytosis of bacteria or polystyrene beads; data not shown) or gene-specific RNAi (Figure 1a). For example, treatment with a drug that prevents the polymerization of filamentous (F-) actin caused Kc_{167} cells to develop long microtubule-rich processes, a morphological change similar to that observed upon treatment with dsRNA corresponding to the gene encoding Cdc42 GTPase. Thus, both cell types could be used with RNAi to assay single-gene functions that contribute to cytoskeletal organization and cell shape.

RNAi assay for cell morphology phenotypes

We set out to conduct parallel RNAi screens with a microscopy-based visual assay to identify genes required for the characteristic round versus flat morphology of Kc_{167} and $S2R^+$ cells, respectively (Figure 1a-c). By labeling actin filaments, microtubules and DNA, it was possible to assay a wide range of cellular behaviors in these cell types, including cytoskeletal organization, cell shape, cell growth, cell-cycle progression, cytokinesis, substrate adhesion and cell viability.

We used dsRNA to *Rho1*, a gene required for cytokinesis [10], to optimize conditions for RNAi in a 384-well plate format. The addition of 0.3 μg *Rho1* dsRNA to cells for a minimum of 3 days in culture generated a penetrant multinucleated cell phenotype (62-100% per imaged field over five wells). Under these conditions, RNAi was effective in both cell types, as judged by the appearance of phenotypes and/or depletion of the targeted gene products. When screening many genes under a single assay condition, several factors could influence the efficiency of RNAi. Given that dsRNA targets the destruction of endogenous mRNA, the efficacy of RNAi and thus the phenotypic strength could reflect gene- and cell-type-specific differences in mRNA levels, the levels and stability of the preexisting protein pool and/or the potency of the chosen dsRNA targeting sequence. In one example, a longer RNAi incubation time of 5 days was necessary to completely deplete the Capulet/Cyclase associated protein, as detected by western blot (although phenotypes affecting F-actin organization were observed by 3 days; data not shown). Thus, it is assumed that the strength or penetrance of RNAi-induced phenotypes observed under one screening condition could vary marginally for any specific gene target or cell type. We reasoned that screening under 'hypomorphic' conditions has the advantage of enabling the effects of gene product depletion to be analyzed rather than its terminal consequences (that is, potential cell lethality). Finally, differences in the phenotypic effects of targeting the same gene with RNAi in two different cell types could reflect true cell-type differences in the function of the targeted genes.

Selection and generation of gene-specific dsRNAs

Screens of RNAi morphological phenotypes required the generation of a dsRNA library. In order to allow an assessment of the overall success of such an RNAi screening approach in *Drosophila* cells, we generated a selected set of 1,042 dsRNAs targeting 994 different genes. The set of genes represented in the library was chosen on the basis of primary sequence to include the vast majority of those predicted to encode signaling components and cytoskeletal regulators that could affect diverse cellular processes (a complete list of the selected categories of predicted gene functions are listed in Table 1; all targeted genes and primer sequences are listed in Additional data file 1, available with the online version of this article). Gene-specific dsRNAs averaging 800 base pairs (bp) in length were generated by *in vitro* transcription, using selectively amplified products from *Drosophila* genomic DNA as templates, then aliquoted into 384-well optical bottom plates for image-based screens (see the Materials and methods section).

The dsRNA collection was selected to enrich for genes encoding classes of central cell regulators, including putative GTPases, GTPase regulators, kinases and phosphatases that can act together as part of signaling pathways to control diverse cellular processes. We also selected cytoskeletal proteins and cell-cycle regulators predicted to be expressed and required in most cells. We favored target selection on the basis of identifiable domains within the primary sequence in order to enrich for both functionally known and uncharacterized genes affecting a wide range

Table 1

RNAi screen results classified by predicted gene function

		Genes identified*							
Gene class†	N	Total		Total S2R+		Total Kc_{167}		Both‡	
Kinase	229	54	18.8%	3	18.8%	2	12.5%	2	12.5%
Miscellaneous	139	16	11.5%	15	10.8%	11	7.9%	10	7.2%
Cytoskeletal	116	17	14.7%	17	14.7%	11	9.5%	11	9.5%
Motor	77	7	9.1%	6	7.8%	3	3.9%	2	2.6%
Phosphatase	72	12	16.7%	10	13.9%	7	9.7%	5	6.9%
GTPase	54	15	27.8%	15	27.8%	6	11.1%	6	11.1%
Transport	48	2	4.2%	1	2.1%	2	4.2%	1	2.1%
Proteolysis	42	7	16.7%	7	16.7%	6	14.3%	6	14.3%
Lipid-associated	38	3	7.9%	3	7.9%	0	0%	0	0%
GEF	32	8	25.0%	7	21.9%	3	9.4%	2	6.3%
PDZ	32	3	9.4%	3	9.4%	1	3.1%	1	3.1%
GAP	31	6	19.4%	5	16.1%	2	6.5%	1	3.2%
SH2/SH3	25	3	12.0%	2	8.0%	1	4.0%	0	0%
Adhesion	23	3	13.0%	3	13.0%	0	0%	0	0%
Cyclase	20	1	5.0%	0	0%	1	9.5%	0	0%
G protein	16	3	18.8%	3	18.8%	2	12.5%	2	12.5%
Total genes	994	160	16.1%	146	14.7%	79	7.9%	65	6.5%

In total, we screened 1,061 wells, 1,042 dsRNAs, 994 genes and found 160 genes with phenotypes. *The number and percentage of genes identified with any RNAi phenotype in duplicate screens. †The total number of genes (*N*) represented in the dsRNA set as defined by amino-acid sequence and Gene Ontology [33] or FlyBase [12] annotation. Each gene was counted in only one category. ‡Genes identified by phenotypes in both Kc_{167} and S2R+ cells.

of processes. Choosing genes from one chromosomal region would be likely to yield fewer visible phenotypes, whereas choosing genes on the basis of their expression in existing cell lines would assume a correlation between expression levels and function.

RNAi screens of cell morphology by image analyses

A phenotypic analysis of Kc_{167} or S2R+ cells treated with each dsRNA and labeled for detection of actin filaments, microtubules and DNA was performed by visual inspection of microscopic images. Defects were considered significant and reproducible when observed in multiple fields of replicate screens by independent observers. All changes observed were annotated using a limited set of phenotypic categories (described in more detail below). Of the genes screened, 16% (160/994) yielded a visible phenotype in Kc_{167} or S2R+ cells (see Table 1 and Additional data file 2, available with this article online). Gene-specific phenotypes were identified in each of the different predicted protein classes screened (Table 1). In addition, genes within any one class exhibited distinct phenotypes, suggesting a high degree of RNAi specificity (for example, genes encoding the GTPases Rho1, Cdc42, R/Rap1 and Ras85D; see below).

Assessment of RNAi screen efficacy

To make screen-wide comparisons of the phenotypes identified, we generated concise phenotypic annotations. As a test of screening efficacy, we evaluated our results by focusing on genes with known or predicted functions in cell-cycle progression in other systems and likely to share conserved functions in *Drosophila* cultured cells; 20 such genes were identified in the screen, 16 of which exhibited an RNAi phenotype consistent with a defect in cell-cycle progression [11] (Figure 2). One group (Profile I) was characterized by an increase in cell size and an altered DNA morphology, indicative of growth in the absence of division. A second group (Profile II) was defined by an increase in the frequency of cells with a microtubule spindle, indicative of a defect in progression through mitosis. Both phenotypic groups could be further subdivided on the basis of additional attributes to generate four distinct sets of functionally related genes that regulate the passage from G1 to S phase (*Cyclin-dependent kinase 4* (*Cdk4*), *Cyclin E*, and the *Dp*), G2 to M phase (*cdc2* and *string*), the onset of anaphase (*fizzy*, *cdc16* and *Cdc27*) and cyclin-dependent transcription (*Cyclin-dependent kinase 9* (*Cdk9*) and *Cyclin T*). Several additional genes were identified with related phenotypes

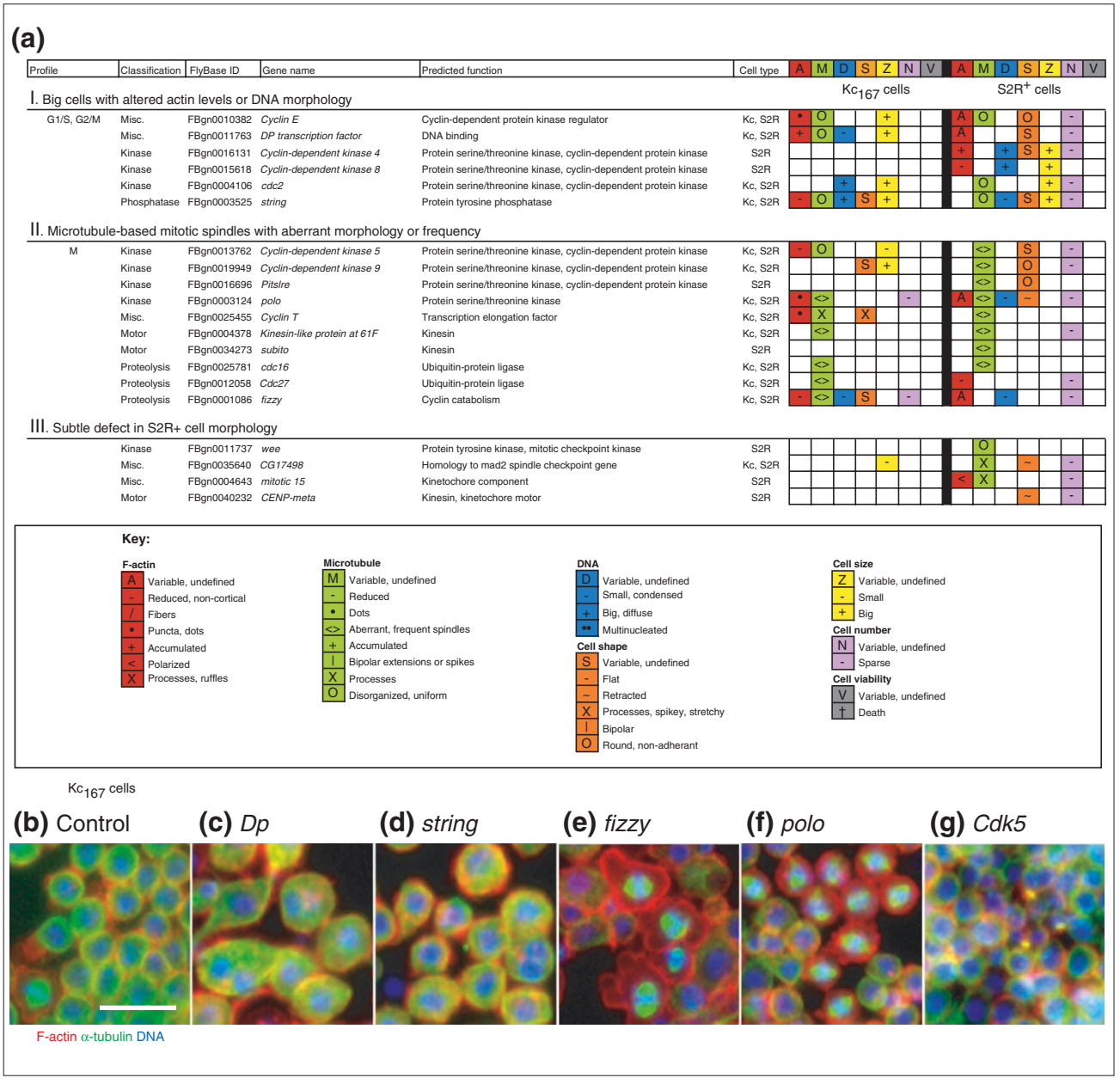

Figure 2

A test of RNAi screen efficacy: identifying genes involved in cell-cycle progression. **(a)** Gene identity and phenotypic annotation for RNAi phenotypes identifying predicted cell-cycle regulators. The 'Profile' column provides a summary of the phenotypic profiles distinguishing sets of genes involved in specific stages of the cell cycle. The 'Classification' column gives a single predicted functional category assigned to each targeted gene on the basis of primary sequence and/or known functional data. The 'FlyBase ID' and 'Gene name' columns are information as annotated at FlyBase [12]. The 'Predicted function' column provides detail on the putative molecular function of each specific gene. 'Cell type' refers to whether the phenotype was observed in Kc_{167} (Kc) and/or $S2R^+$ (S2R) cells. Profile I: RNAi phenotypes resulting in an increase in cell size, uniform or disorganized microtubules, irregular cell shapes and decreased cell numbers identified genes involved in cell-cycle progression through G1 to S and G2 to M stages. Phenotypes were further distinguished on the basis of levels of F-actin accumulation and DNA morphology. Profile II: RNAi phenotypes resulting in aberrant morphology or increased frequency of microtubule-based mitotic spindles identified genes involved in mitosis. Profile III: RNAi phenotypes observed in $S2R^+$ cells identified additional genes with putative roles in cell cycle/mitosis progression. **(b-g)** Kc_{167} cells stained for F-actin (red), α-tubulin (green), DNA (blue), imaged using automated microscopy and scored visually. (b) Control. (c,d) Profile I: *Dp* and *string* RNAi resulting in big cells. (e,f) Profile II: *fizzy* and *polo* RNAi resulting in increased frequency of cells with mitotic spindles. (g) *Cdk5* RNAi resulting in smaller cells and disorganized microtubules (and increased spindles in $S2R^+$ cells; not shown). Scale bar, 30 μm.

(see Additional data file 2). For example, dsRNAs targeting a predicted *Cyclin-dependent kinase 8* (*Cdk8*) and a novel gene *CG3618* both resulted in large cells with aberrant DNA morphology (data not shown), similar to cells with targeted *cdc2* or *string*. It is therefore possible to use visual RNAi screens to functionally characterize a large set of genes and, by grouping genes according to morphological criteria, to identify functional modules.

For other cellular processes, limited *Drosophila* genetic data are available with which to measure the success of the screens. We discovered, however, many examples of RNAi-induced phenotypes that are consistent with the previously predicted or described gene function in another assay system (examples discussed below). Importantly, in one-third of all cases, an RNAi-induced phenotype identified a previously uncharacterized gene that lacked a corresponding mutant allele in *Drosophila* (at least 51/160 genes; see Additional data file 2) [12]. This shows that RNAi screens represent a valuable addition to classical *Drosophila* genetic screens.

Table 2

RNAi screen results classified by annotated phenotype

	Genes identified*			
Phenotypic class†	Total	Total S2R+	Total Kc_{167}	Both‡
Cell shape	105	93	32	20
F-actin organization	94	74	50	30
Microtubule organization	71	48	37	14
Decreased cell density	66	62	8	4
Cell size	48	25	33	10
DNA morphology	27	17	22	12
Cell viability	6	3	4	1
Total phenotypes	417	322 (77%)	186 (44%)	91 (22%)
Total genes	160	146 (91%)	79 (49%)	65 (41%)

*The number of genes categorized with a specific RNAi phenotype in duplicate screens. †The major classes of RNAi phenotypes. Individual genes with multiple phenotypes were counted within each of the phenotypic classes scored. ‡Genes identified by a defect assigned to the same phenotypic class in both cell types.

Classification of RNAi cell morphology phenotypes

We detected a broad spectrum of distinct defects in cytoskeletal organization and cellular morphology, including subtle effects in the localization and level of actin filaments and microtubules (see Table 2, Figure 3 and Additional data file 2 with the online version of this article). To classify the results, phenotypes were scored using defined descriptions assembled under one of seven major categories, denoting visible defects in actin filaments, microtubules, DNA, cell shape, cell size, cell number and cell viability (Table 2). We were able to further define subcategories that describe specific morphological attributes (see Materials and methods section for more details). Some descriptions were interdependent and therefore redundant; for example, cell shape was determined by a combined assessment of the actin and microtubule organization.

Using this system, a total of 417 phenotypic annotations were assigned to 160 genes, ranging from zero up to six annotations per gene in one cell type (Table 2, Figure 4). A comparison between the two RNAi screens revealed that 41% (65/160) of the genes were identified with phenotypes in both Kc_{167} and S2R+ cell types. This overlapping set identified many genes that are known to control important cell-biological functions common to all cell types, such as cell-cycle progression and cytokinesis, and genes that may reflect a hemocyte origin (Figure 2 and see below). In comparing the two cell types, nearly twice as many of the genes were found to have a detectable RNAi phenotype in S2R+ cells (146/160 genes, or 91% of the total) as in Kc_{167} cells (79/160; 49% of the total). Genes identified in S2R+ cells also had a greater mean number of phenotypic annotations assigned to them (2.0) than in Kc_{167} cells (1.2; see Figure 4). This was due in part to the ease of detecting overt phenotypes in the larger S2R+ cells but may also indicate a difference in the number of genes required to maintain a flat versus a round cellular morphology (see below). Interestingly, the relative importance of a gene in the two cell types, as determined by RNAi, did not strictly correlate with the relative levels of expression. Furthermore, RNAi was shown to deplete the protein in cases in which there was no measurable phenotype in our assay (see below; and data not shown).

We also noted cases in which morphological defects were accompanied by a decrease in cell number. An RNAi-induced phenotype was accompanied by a notable decrease in cell number (estimated as fewer than half the normal number of cells per image) in 43% of cases (68/160 genes; see Additional data file 2 with the online version of this article). Less than 1% of the genes screened caused a catastrophic reduction in cell number (an estimated fewer than 100 cells per image) three days after the addition of dsRNA (6/994 genes, listed as having a cell viability defect in Additional data file 2). One example of this class of genes was a known inhibitor of apoptosis, D-IAP1 [13]. These data demonstrate that under these conditions, severe cytotoxicity is not a major obstacle for cell-based RNAi screens, even if many of the genes are essential for *Drosophila* development.

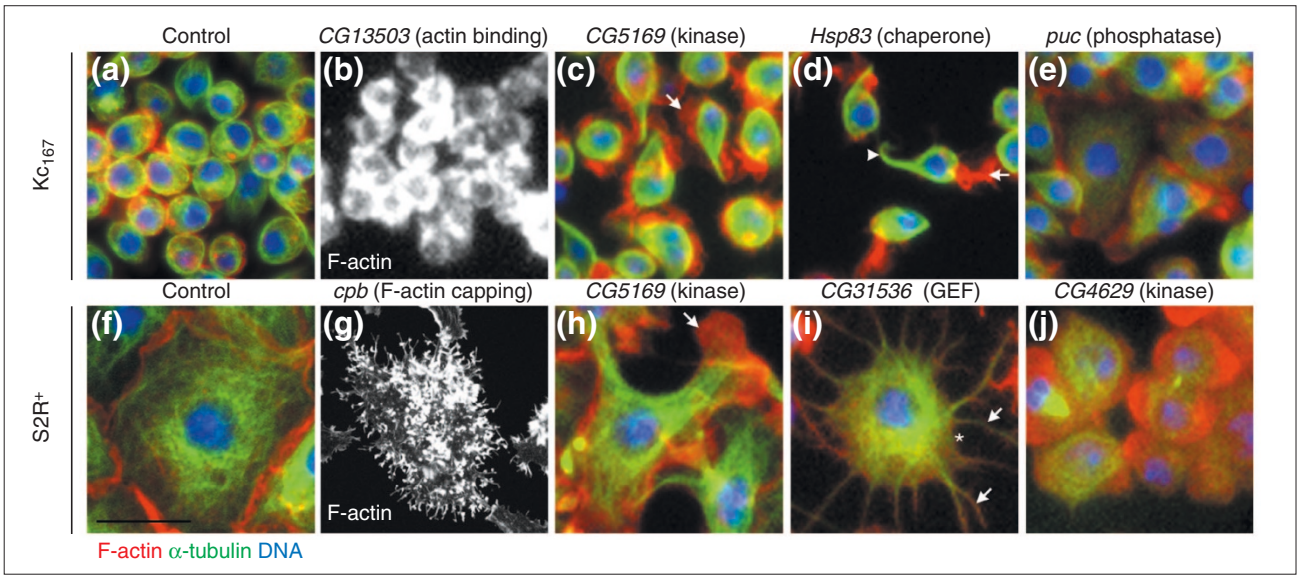

Figure 3
RNAi screens identified a wide range of gene functions based on diverse morphological phenotypes. Cells were stained for F-actin (red), α-tubulin (green) and DNA (blue), imaged using automated microscopy and scored visually. **(a)** Control Kc_{167} cells. **(b-e)** Kc_{167} cells with RNAi phenotypes. **(f)** Control $S2R^+$ cells. **(g-j)** $S2R^+$ cells with RNAi phenotypes. (b) F-actin accumulation; *CG13503* RNAi (encoding a predicted WH2-containing actin-binding protein). (c,h) Flatter, polarized cells with actin-rich lamellipodia (arrows); *CG5169* RNAi (a predicted kinase). (d) Opposing protrusions rich in F-actin (arrow) or microtubules (arrowhead), *Hsp83* RNAi (chaperone). (e) Flat cells; *puckered* RNAi (JNK phosphatase). (g) Widely-distributed F-actin puncta; *capping protein beta* RNAi (component of CapZ). (i) Radial protrusions (arrows) and reduced cortical actin (asterisk); *CG31536* RNAi (predicted Rho-GEF with FERM domain). (j) Rounder cells, decreased in size; *CG4629* RNAi (predicted kinase). Scale bar, 30 μm.

RNAi phenotypes with common cytoskeletal defects

Changes in actin organization and cell shape were the most commonly observed phenotypes (94 and 105 out of 401 phenotypes, respectively). In some instances, specific dsRNAs led to defects in F-actin with related morphological consequences in both Kc_{167} and $S2R^+$ cells (22 genes). For example, both cell types displayed RNAi phenotypes characterized by an elevated accumulation or a polarized (asymmetric or uneven) distribution of F-actin (13 genes). These phenotypes identified genes encoding proteins thought to limit the rate of actin-filament formation [14], such as *twinstar* (encoding cofilin) and *capping protein beta*, as well as previously uncharacterized *Drosophila* genes, such as *Pak3* and *CG13503* (Figure 3b,g). Conversely, dsRNAs targeting several known regulators of actin-filament formation compromised cortical F-actin in both cell types (9 genes). In addition, actin-rich protrusions were observed in both cell types following dsRNA targeting of *CG5169* (Figures 3c,h), a *Drosophila* gene encoding a homolog of a *Dictyostelium* kinase thought to regulate severing of actin filaments [15]. Thus, one class of cytoskeletal regulators has similar functions in two morphologically distinct cell lines, irrespective of their characteristic shape. In addition, a significant proportion of the genes implicated in cell-cycle progression (65%) or cytokinesis (50%) exhibited similar RNAi phenotypes in both cell types.

RNAi phenotypes affecting distinct cell shapes

To identify genes that specify different cell shapes, we focused on morphological phenotypes that were restricted to either Kc_{167} or $S2R^+$ cells. Indeed, 78% of the morphological phenotypes observed were detected in only one of the two cell types. Kc_{167} cells frequently adopted a unique, bipolar spindle shape in response to specific dsRNAs (21 genes), reminiscent of the cell-shape change induced by actin-destabilizing agents or ecdysone (Figure 1). This shape change was usually associated with the formation of discrete F-actin puncta and opposing microtubule-rich processes and was seen in cells treated with dsRNAs targeting genes known to promote actin-filament formation (such as those encoding Cdc42 and SCAR) [14] and others known to affect microtubules (for example, *par-1*) [16]. These observations suggest that actin filaments and microtubules play antagonistic roles in Kc_{167} cells, with the contractile actin cortex opposing the formation of microtubule-based processes. Although Kc_{167} cells exhibited a marked tendency to take on a bipolar morphology, various gene-specific manifestations of this phenotype were distinguishable. For example, a single, microtubule-rich extension formed directly opposite from a single, large, actin-rich protrusion in Kc_{167} cells treated with dsRNA targeting the gene for the Hsp83 chaperone (Figure 3d). In addition, a large and flat bipolar morphology

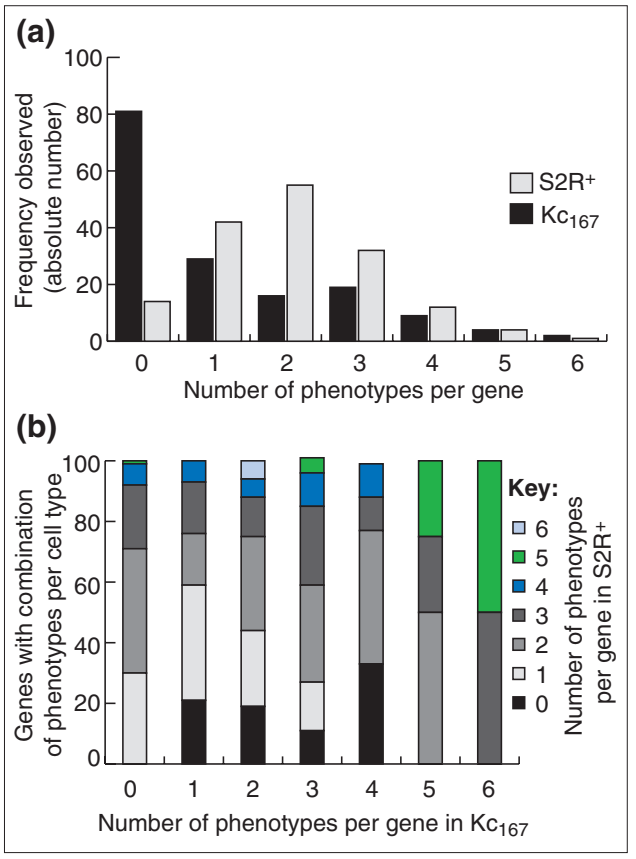

Figure 4
The distribution of phenotypic annotations. **(a)** Frequency of genes associated with a number of different RNAi phenotypes (0-6) per cell type. Phenotypes refer to those identified by seven major annotation categories. From 0 up to 6 phenotypes per gene were observed; '0' indicates those genes without detectable phenotypes in the one cell type (but were detected in the other). The set included all 160 genes identified by an RNAi phenotype in each of either S2R+ (gray) or Kc_{167} (black) cell types. **(b)** The percentage of genes associated with a certain combined phenotypic annotation in both cell types screened. The percentage is the number of genes identified with 0 to 6 phenotypic annotations in Kc_{167} cells (normalized to 100%) that were also associated with 0 to 6 phenotypic annotations in S2R+ cells (colored fractions of columns; see the key).

was induced in Kc_{167} cells treated with dsRNAs targeting the *puckered* gene encoding JNK phosphatase (Figure 3e), *CG7497*, encoding a predicted G-protein-coupled receptor kinase, and the *Pten* gene encoding phosphatidylinositol (3,4,5)-trisphosphate (PIP_3) 3-phosphatase (see below).

One major behavioral difference between the two cell types used in this study is the ability of S2R+ cells to adhere to and spread over the substratum. As a result, subtle changes in cytoskeletal organization could be visualized in S2R+ cells, such as polarized (uneven) F-actin accumulation (in response to dsRNA targeting *Abl*-encoded kinase), actin stress-fiber formation (the *RhoL*-encoded GTPase) and the loss of cortical actin filaments (dsRNA targeting *CG31536*, encoding a predicted Rho guanine-nucleotide exchange factor (GEF) with a FERM domain; Figure 3i). Of particular interest were genes required for the spreading process characteristic of S2R+ cells. S2R+ cells rounded up and detached from the plate in response to dsRNAs targeting 37 different genes, 20 (54%) of which had no visible effect on Kc_{167} cells. Four genes identified in this way had known functions in cell-matrix adhesion [17] (see Figure 5c), including an enigmatic adhesion molecule that contains an integrin-ligand RGD sequence (*Tenascin-major*) [18], both α and β integrin subunits (*inflated* and *myospheroid*) and a focal-adhesion cytoskeletal anchor (*talin*) [19], as well as focal adhesion kinase (*FAK56D*, with a slightly different defect in cell spreading). This set also included novel genes (*CG4629*, encoding a predicted kinase; Figure 3j). The remaining 17 genes that, by RNAi, affected both S2R+ cell spreading and Kc_{167} cell morphology may identify those that indirectly affect the cell-adhesion process (for example, S2R+ cells rounded up as a consequence of RNAi-induced arrest in mitosis; Figures 2 and 6).

The set of genes identified by RNAi defects in cell spreading suggested that S2R+ cells utilize focal adhesion complexes to flatten on the substrate. An implication of this finding is that Kc_{167} cells may be unable to spread on the substrate because they fail to express adhesion-complex components. Surprisingly, quantitative PCR (qPCR) of reverse-transcribed mRNA revealed a 2.4-fold enrichment of *βPS integrin* (*mys*) expression in Kc_{167} cells versus S2R+ cells (adjusted cross-point difference of 1.2 cycles; see Materials and methods section; data not shown). Furthermore, βPS integrin/Mys protein was detected in both cell types, with slightly elevated levels in untreated Kc_{167} cells versus S2R+ cells, and similarly depleted in both upon treatment with *mys* dsRNA (Figure 7). We extended the analysis to other adhesion-complex components identified in the screen and discovered by qPCR that both *α-integrin* (*if*) and *Rap1* (*R*) were also expressed in Kc_{167} cells, although at slightly lower levels than in S2R+ cells (adjusted cross-point differences of 1.0 and 0.3 cycles, respectively). In contrast, S2R+ cells exhibited a nearly 4.6-fold enrichment of *talin* expression relative to that in Kc_{167} cells (adjusted cross-point difference of 2.3 cycles). Moreover, Mys levels were sensitive to the loss of *Rap1* by RNAi in S2R+ cells (Figure 7). This analysis demonstrated that although many of the same adhesion complex components are expressed in both the round Kc_{167} and spread S2R+ cells, the genes function differently in the two cell types, so that integrin-mediated adhesion has little impact on the morphology of Kc_{167} cells.

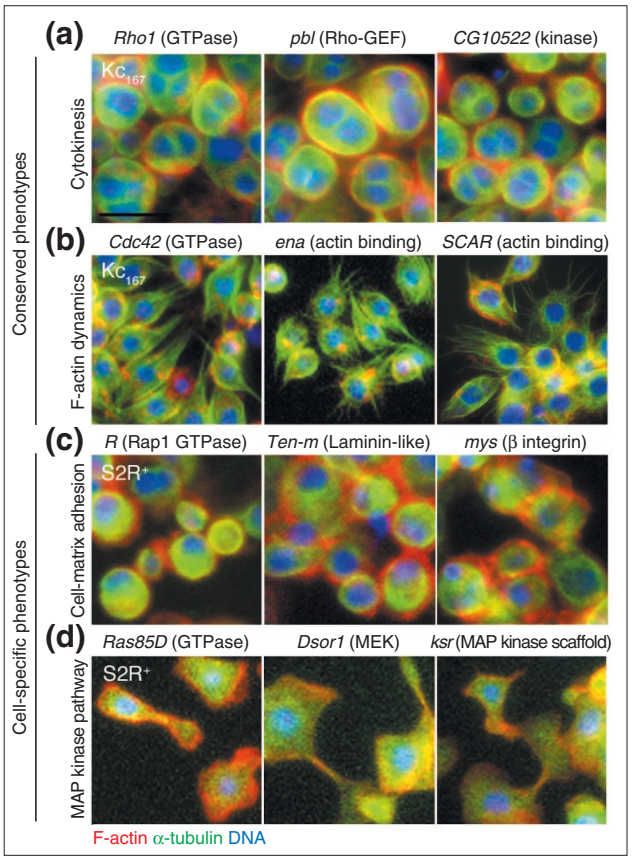

Figure 5
Similar phenotypic profiles identified genes in pathways and protein complexes. Cells were stained for F-actin (red), α-tubulin (green) and DNA (blue). Distinct phenotypes were observed with dsRNAs targeting different members of the same functional family (for example, GTPases, in the left panels). **(a,b)** Phenotypes observed in both cell types. (a) RNAi-induced binucleate cell phenotypes identified genes required for cytokinesis, including *Rho1* (encoding a GTPase), *pebble* (a Rho-GEF) and *CG10522* (a predicted citron kinase). Kc_{167} cells are shown. (b) RNAi resulting in loss of actin filaments from the cell cortex identified regulators of actin-filament formation, including *Cdc42* (GTPase), *enabled* (actin-binding protein) and *SCAR* (actin-binding, Arp2/3 regulator). Kc_{167} cells (shown) also formed microtubule extensions and a polarized cell shape. **(c,d)** Some phenotypes were unique to one cell type. (c) RNAi resulting in round, non-adherent $S2R^+$ cells identified genes required for cell-matrix adhesion, including *Roughened* (a Rap1 GTPase), *Tenascin-major* (an adhesion protein with a laminin domain) and *myospheroid* (β integrin). (d) An RNAi-induced amorphous $S2R^+$ cell phenotype identified genes in the mitogen-activated protein (MAP) kinase pathway, including *Ras85D* (a GTPase), *Downstream of raf1* (a MAP kinase kinase, or MEK) and *kinase suppressor of Ras* (a MAP kinase scaffold protein).

Furthermore, Kc_{167} cells adhered but remained round even when plated on an adhesive concanavalin A substrate that induced round S2 cells to flatten [20] (data not shown), although Kc_{167} cells do flatten when actin-filament formation is compromised (Figure 1). Thus, spreading of *Drosophila* cells probably requires both integrin-mediated adhesion and reorganization of cortical F-actin. This is supported by the fact that $S2R^+$ cells rounded up when treated with *cofilin* dsRNA because of an accumulated excess of cortical actin filaments. Integrins may, therefore, function to mediate substrate adhesion in both cell types, while the levels of additional gene products (such as talin, cofilin and phosphoinositide (PI) 3-kinase activity) determine whether or not the cell will spread.

Genes with common phenotypes share morphogenetic functions

The results from RNAi screens in both cell types were combined to generate a phenotypic profile for each gene. Genes with similar phenotypic profiles were involved in common morphogenetic functions, as indicated by several distinct sets of genes known to interact in pathways or complexes. In both cell types, dsRNAs specific for the *pebble* gene encoding a Rho-GEF, the *Rho1* gene encoding a GTPase, and the *CG10522* gene encoding citron kinase led to enlarged cells with multiple nuclei, indicative of a failure to form and constrict the actin contractile ring necessary for cytokinesis (Figure 5a). While *Rho1* and *pebble* (and five other identified genes; see Figure 6) have already been shown to function in *Drosophila* cytokinesis [3,10], we identified *CG10522* in the RNAi screen as a potential novel Rho1-effector required for cytokinesis [21]. RNAi targeting of members of a different group of genes resulted in a profound loss of actin filaments in both cell types, identifying known regulators of F-actin formation. In Kc_{167} cells, dsRNAs targeting the *Cdc42*-encoded GTPase, *enabled*-encoded actin-binding protein, and *SCAR*-encoded regulator of Arp2/3 complex [14], each led to a reduction in F-actin, the appearance of microtubule-rich protrusions and cell flattening (Figure 5b). In $S2R^+$ cells, RNAi of *Cdc42*, *enabled* or *SCAR* similarly reduced the levels of F-actin, compromising the ability to form lamellipodia (as in Figure 3i, and data not shown). Ena protein was effectively depleted upon *ena* RNAi in both cell types (Figure 7).

The screen profiles also identified clusters of genes with phenotypes unique to a single cell type, such as the set of matrix-adhesion genes required for $S2R^+$ cell spreading, as noted above (Figure 5c). Three dsRNAs caused $S2R^+$ cells to assume a unique, amorphous shape. This striking phenotype identified *Ras85D*, *Downstream of Raf1* (encoding mitogen-activated protein (MAP) kinase kinase, or MEK) and *kinase suppressor of Ras*, all interacting components of the well-characterized MAP kinase signaling pathway [22] (Figure 5d). Thus, on the basis of phenotype alone, groups of genes were identified that function in the same cellular process, complex or pathway. In classic *Drosophila* genetic

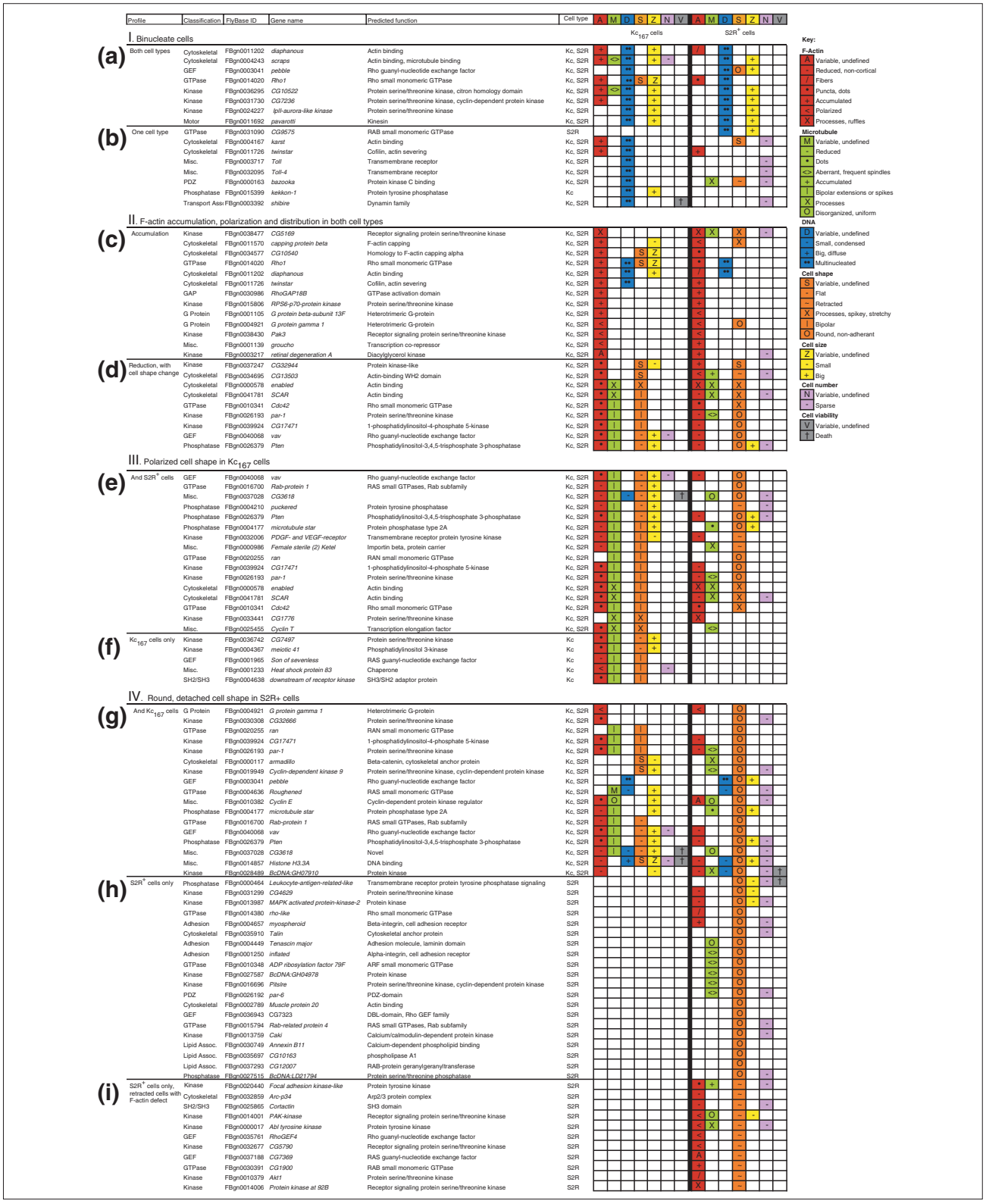

Figure 6 *(see legend on the next page)*

screens a similar logic was used to group genes on the basis of common mutant cuticle phenotypes, identifying genes that act together to control different aspects of embryonic development [23].

A co-RNAi screen identifies modifiers of the *Pten*-dsRNA-induced cell shape phenotype

Part of the success of using *Drosophila* as a model genetic system has relied upon modifier screens to identify novel components acting in related processes or molecular pathways of interest [24]. Using an analogous approach in cell culture, we designed an RNAi screen to identify genes that modify a specific RNAi-induced cell-shape change. *Pten*, a human tumor suppressor gene, is a lipid phosphatase that dephosphorylates PIP_3, acting in opposition to PI 3-kinase [25] to control many cellular processes including growth, adhesion, migration and apoptosis [26]. In the initial screen, *Pten* RNAi was found to polarize Kc_{167} cells, inducing microtubule extensions and a flattened, bipolar shape (Figure 8b). A lower concentration of *Pten* dsRNA caused a visible but less severe asymmetric microtubule phenotype (Figure 8c) that was used for a co-RNAi screen to identify *Pten* modifiers.

By screening for dsRNAs that modified the asymmetric microtubule distribution seen in response to *Pten* RNAi, 20 of the 229 dsRNAs targeting predicted kinases were identified as visible suppressors of this phenotype. These included dsRNAs corresponding to seven genes that were not identified in screens in untreated Kc_{167} cells: *Akt1*, *CG31187*, *LIM-kinase 1*, *MAP kinase activated protein-kinase 2*, *Pi3K92E*, *slipper* and *wee*. Importantly, two of these encode known positive regulators of the pathway: *Pi3K92E* and *Akt1* [6] (Figure 8d,e). One suppressor, *CG31187*, encodes a predicted diacylglycerol kinase that may act directly in the phosphoinositide cycle [27]. It is possible that other genes identified as RNAi suppressors may rescue the *Pten*-morphology phenotype indirectly by modifying actin-filament organization (*LIMK1* [28]). These results demonstrate that modifier screens, like those used to identify new components of specific pathways in classical genetic systems, can now be carried out in cell culture using RNAi-screening technology.

Conclusions

Despite a limited knowledge of the molecular mechanisms used to maintain the morphology of *Drosophila* cells in culture, we have identified over 100 genes with visible loss-of-function phenotypes that affected specific aspects of metazoan cytoskeletal organization, cell-cycle progression, cytokinesis and cell shape. While both Kc_{167} and $S2R^+$ cells appear to use a similar set of genes to regulate actin filaments at the cell cortex and for cytokinesis, $S2R^+$ cells spread on the substrate using integrin-mediated adhesion, and Kc_{167} cells require proper control of the PI 3-kinase pathway to maintain their round shape. Furthermore, the functional consequences of a reduction in the expression of an individual gene did not correlate with its level of expression in the two cell types. It is more likely that gene function is determined by the network of functional interactions of a large number of proteins. Thus, our analysis has generated a genetic description of two cell types that reveals potential mechanisms through which their contrasting cell shapes might be generated. The same technology can be easily adapted using modified cell lines or conditions to a wide variety of cell-based studies and on a greater genomic scale. Comparisons between diverse RNAi screens will be invaluable in illuminating the complexities in the ways in which sets of genes can functionally interact to generate different cell behaviors. Significantly, RNAi screens bring systematic reverse genetics to cell culture, facilitating comprehensive functional analyses of cell-biological processes.

Materials and methods

Selection of gene targets and primer pairs

The set of genes represented in the RNAi library was chosen to include the vast majority of those encoding predicted signaling components and cytoskeletal regulators. Genes were

Figure 6 *(see figure on the previous page)*
RNAi profiles identify known and novel genes with related morphogenetic functions. Table headings are as defined as in Figure 2. **(a,b)** Profile I: binucleate cells that identified genes required for cytokinesis, as detected either in (a) both cell types or (b) a single cell type. **(c,d)** Profile II: F-actin phenotypes observed in both cell types identified genes with potentially conserved roles in F-actin dynamics. (c) Increased or polarized (uneven) accumulation of F-actin identified genes with potential roles in F-actin capping, severing or depolymerization. (d) Reduced F-actin and altered cell shape identified genes with potential roles in F-actin polymerization. **(e,f)** Profile III: a common RNAi phenotype observed in Kc_{167} cells was a change from round to spindle-shaped, with the formation of F-actin puncta and microtubule extensions. (e) Cases with phenotypes also observed in $S2R^+$ cells identified genes involved in F-actin and microtubule regulation. (f) Cases with phenotypes observed only in Kc_{167} cells identified components of receptor signaling pathways. **(g-i)** Profile IV: RNAi phenotypes resulting in round, detached $S2R^+$ cells. (g) Phenotypes detected in both $S2R^+$ and Kc_{167} cells identified genes with probable indirect effects on cell adhesion and spreading, including roles in the cell cycle and cell viability; (h) RNAi phenotypes specific for $S2R^+$ cells identified genes that may distinguish the flat $S2R^+$ cell morphology, including genes encoding cell-matrix adhesion components. (i) Genes identified by a related RNAi phenotype, resulting in retracted (unspread but flat) $S2R^+$ cells .

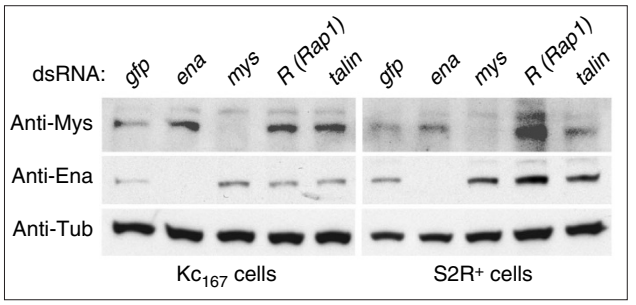

Figure 7
Levels of gene expression do not necessarily correlate with gene function. Immunoblot detection of anti-βPS-integrin (Mys, top panels) and anti-Enabled (Ena, middle panels) after 3 days RNAi. Columns represent Kc_{167} cells (left) and $S2R^+$ cells (right) treated with different dsRNAs (*gfp*, *ena*, *mys*, *R*, *talin*). Both cell types expressed Mys and Ena in cells treated with a nonspecific dsRNA. The respective proteins were completely and specifically depleted by treatment with *mys* or *ena* dsRNAs. Anti-α-tubulin (bottom panels; Tub) shows a loading comparison.

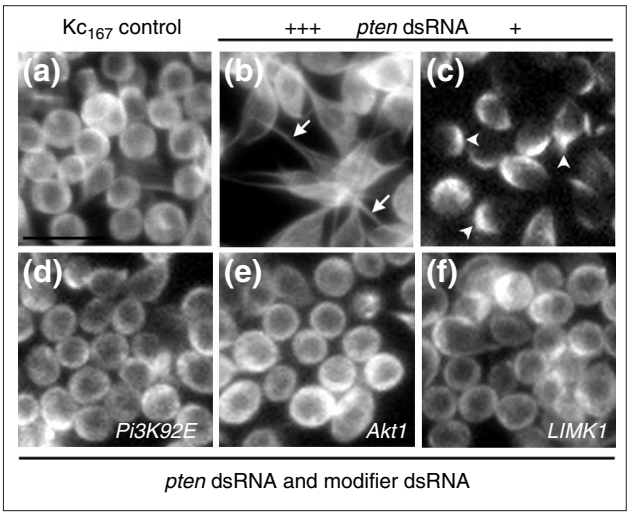

Figure 8
A co-RNAi screen for modifiers of *Pten*-dsRNA phenotype. Microtubules are visualized by α-tubulin immunostaining. **(a)** Control Kc_{167} cells exhibited normal, round morphology. **(b)** In response to *Pten* dsRNA at the same concentration as the original screening conditions, Kc_{167} cells were bipolar and spindle-shaped with microtubule extensions (arrows). **(c)** In response to a relatively low concentration of *Pten* dsRNA, the conditions used for the modifier screen, Kc_{167} cells exhibited a less pronounced phenotype with asymmetric microtubule accumulation (arrowheads). Specific dsRNA suppressors of the *Pten*-RNAi-induced cell shape restored the normal, round cell morphology and microtubule organization, identifying **(d)** *Pi3K92E*, **(e)** *Akt1* and **(f)** *LIMK1*.

selected on the basis of a combination of predictions using annotations in the FlyBase [12] and Berkeley *Drosophila* Genome Project (BDGP) databases [29] and by BLAST searches for orthologs of known genes with functional domains via NCBI/GenBank [30]. The selected genes were categorized according to one of the following predicted protein functions or domains: adhesion molecules, adenylate and guanylate cyclases, cytoskeletal proteins and binding proteins (such as proteins with WH and FERM domains), G proteins, GTPase-activating proteins (GAPs), GEFs, GTPases, kinases, lipid-associated proteins (such as phospholipases or proteins containing PH and PX domains), miscellaneous proteins (such as transcription factors, PI phosphotyrosine-binding domains and cell-cycle regulators), motors (such as dynein, kinesins and myosins), PDZ-domain-containing proteins, phosphatases, proteins involved in proteolysis (such as ubiquitin-conjugating enzymes and ligases), proteins containing SH2 or SH3 domains and vesicle-transport-associated proteins (such as SNAREs, SNAPs and dynamins). A complete list is presented in Additional data file 1 with the online version of this article.

Primer sequences were predicted using genomic and annotation data from the BDGP Release 1 [4] with the Primer3 software [31]. Primers were preferentially selected to span predicted exonic sequences if confirmed by the existence of expressed sequence tag (EST) or protein homology data. Electronic PCR [32] was used to select amplification products from genomic sequence between 200 and 1,800 bp in length and possessing < 21 bp of exact match with any other predicted or confirmed transcript sequence. A smaller PCR product size was selected if the genomic sequence corresponded to > 500 bp coding sequence. PCR primers could only be predicted within the most proximal half of the intergenic sequence of each gene.

Generation of dsRNA

OregonR genomic DNA was PCR-amplified using Taq (PerkinElmer, Foster City, USA) with 5 μM each primer in 96-well plates (Tetrad from MJ Research Inc., Waltham, USA; 92°C for 1 min, 34 cycles of 92°C for 20 sec, 54°C for 40 sec, 72°C for 4 min, then 72°C for 3 min and held at 4°C), ethanol precipitated, washed, vacuum dried and resuspended in 7 μl DEPC-treated 100 mM Tris-HCl, 0.1 mM EDTA. Separate T3 and T7 *in vitro* transcription reactions were conducted (T3 and T7 MEGAscript; Ambion, Austin, USA) using 1.5 μl PCR product per well, incubated at 37°C for 4.5 h, and diluted with 47 μl of RNase-free water. T3 (50 μl) and T7 (50 μl) reaction mixes were combined, purified using RNeasy 96 Kits and a QIAvac 96 vacuum manifold (QIAGEN, Valencia, USA), soaked twice for 2 min and eluted in 80 μl RNase-free water. To anneal T3 and T7 single-strand RNAs, 50 μl purified RNA was mixed with 10 μl 6× buffer (40 mM KPO_4 pH 7.5, 6 mM K-citrate pH 7.5,

4% PEG 6000) and heated in a PCR block at 68°C for 10 min and 37°C for 30 min. Purified dsRNA and remaining non-annealed mixes were stored in 96-well plates at -70°C. For screens, an average of 0.3 μg dsRNA in 3 μl was transferred from stock plates to 384-well black-sided, tissue-culture-treated optical bottom-assay plates (Corning, Acton, USA) using a multichannel pipette or a CyBio robot (CyBio US Inc., Woburn, USA).

Cell cultures

Kc_{167} cells and S2R+ cells were grown in Schneider's medium (Invitrogen, Carlsbad, USA) with 10% heat-inactivated fetal bovine serum (JRH Biosciences, Fenexa, USA) and penicillin-streptomycin (Sigma, St Louis, USA) at 24°C in treated culture flasks (Falcon from BD Biosciences, Bedford, USA). S2R+ cells were removed from culture flasks using Trypsin-EDTA (Invitrogen).

RNAi and cell staining

RNAi was performed as described [6]. Briefly, 1.2×10^4 cells in 10 μl serum-free Schneider's medium were added to dsRNAs in 384-well assay plates using a Multidrop384 liquid dispenser (Thermo Labsystems, Franklin, USA), centrifuged at 1,200 rpm for 1 min, then incubated at room temperature for 30 min before adding 30 μl more medium with serum by MultiDrop. Cells were grown for 3 days at 24°C. In the RNAi-modifier screen, 0.1 μg *Pten* dsRNA in 3 μl was added to each assay-well before plating cells. Cells were processed using the MultiDrop dispenser and a multichannel manifold (Drummond Scientific, Broomall, USA). Cells were fixed for 10 min in 4% formaldehyde (Polyscience, Niles, USA) in phosphate-buffered saline (PBS), washed twice in PBS with 0.1% Triton-X-100 (PBST), stained overnight at 4°C with FITC-conjugated anti-tubulin (DM1A; Sigma) and TRITC-phalloidin (Sigma) in PBST with 3% bovine serum albumin, stained for 10 min in PBS with 4',6-diamidino-2-phenylindole, dihydrochloride (DAPI; Sigma) and washed in PBS.

Autoscope image acquisition

Fluorescent images of cells in 384-well plates were acquired using an automated Nikon TE300 microscope with a 20× objective and HTS MetaMorph software (Universal Imaging, Downington, USA) running an automated Mac5000-driven stage, filter wheel and shutter (Ludl Electronic Products, Hawthorne, USA), an automated Pifoc focusing motor (Piezo Systems Inc., Cambridge, USA) and an Orca-ER cooled-coupled device camera (Hamamatsu Corporation USA, Bridgewater, USA). Images were also acquired using a similar automated microscope with a Prior stage and controller (instrument kindly shared by the Institute for Chemistry and Cell Biology, Harvard Medical School). Automated focusing was performed on DAPI-stained DNA. Images from UV, TRITC, and FITC channels were then collected within the same plane using preset exposures and a binning of 2 (640 w × 512 h pixels). Images from two different sites within each well were collected, representing around 12% of the total area. Multichannel images were combined as an RGB overlay within a stack of images for each plate.

Image annotation

Images from each channel and combined RGB images were visually scored independently by two researchers (B.B. and A.K.). Annotations assigned to each of the different sites imaged within every well were exported from MetaMorph into Excel spreadsheets. Phenotypes observed in multiple fields of replicate screens by independent observers were considered for further analysis. All visible phenotypes observed for an estimated majority of imaged cells per dsRNA treatment were recorded. Phenotypes were classified into one of seven major categories denoting visible defects in actin filaments, microtubules, DNA, cell shape, cell size, cell number and cell viability. Some descriptions were interdependent and therefore occasionally redundant: for example, cell shape was determined by an overall assessment of the actin and microtubule organization. Further subcategories were used to describe specific morphological attributes, although potentially subtle differences were still distinguishable between specific dsRNA phenotypes grouped within the same category. Specific categories included the following.

F-actin

(a) Variable or undefined; (b) reduced levels or non-cortical (F-actin not apparent at the cell cortex, with diffuse or low levels of staining); (c) fibers (the appearance of spikes of F-actin away from the cortex, within the cell body); (d) puncta or dots (smaller and bigger accumulations within the cytoplasm, respectively); (e) accumulated (elevated levels and/or expanded at the cortex); (f) polarized (asymmetric distribution of actin at the cortex, usually fewer but larger accumulations than puncta or dots); (g) processes or ruffles (spiky or broad actin-rich protrusions, reminiscent of filopodia and lamellipodia).

Microtubules

(a) Variable or undefined; (b) reduced levels; (c) dots (as described for F-actin); (d) aberrant or frequent mitotic spindles (unusually formed or sized spindles and/or an increased frequency of spindles); (e) accumulated; (f) bipolar extensions or spikes (elongated microtubule bundles emanating as one to two opposing radial cell protrusions); (g) processes (multiple radial protrusions of microtubule bundles); (h) disorganized, uniform (a microtubule network throughout the cytoplasm, no longer with stronger staining of the perinuclear array).

DNA
(a) Variable or undefined; (b) small or condensed; (c) big or diffuse (abnormal size was estimated); (d) multinucleated cells.

Cell shape
(a) Variable or undefined; (b) flat; (c) retracted (pertains to S2R+ cells that remained flat but less well or less evenly spread, based on the shape and length of the cell edge and an estimate of the spreading area); (d) processes, spiky or stretchy (a description of the cell edge, in combination with F-actin and microtubule organization); (e) bipolar (pertains to Kc_{167} cells with a polarized axis, with varying degrees of lengthening ranging from lemon shapes to elongated spindle shapes); (f) round or nonadherent (pertains to S2R+ cells that were no longer flat).

Cell size
(a) Variable; (b) small; (c) big (based on estimated size).

Cell number
(a) Variable; (b) sparse (having an estimated less than half of the normal cell confluence of approximately 1,000 cells per field).

Cell viability
(a) Death (fewer than an estimated 100 cells per field).

Molecular assays

Cells were plated at 10^6 cells per ml in 6-well plates with or without 15 μg dsRNA (results shown are either with *gfp, mys, if, Rap1* or *talin*), as described above. After 3 days, cells in duplicate wells were processed for either protein or mRNA analyses. For protein detection on western blots, cells were washed, collected, resuspended in 75 μl lysis buffer (50 mM Tris, pH 7.5; 150 mM NaCl; 1 mM EDTA; 1% NP40; 0.5% DOC; 10% SDS; 10 mM NaF; 1 mM NaOV; protease inhibitors), incubated on ice for 15 min and spun at 4°C for 10 min before loading 10-12 μl supernatant with 2-mercaptoethanol to run on a 10% Tris-HCl polyacrylamide electrophoretic gel (BioRad, Hercules, USA). Semi-dry transfer to nitrocellulose membrane was probed with rabbit anti-Myospheroid (185E; gift of R. Hynes), mouse anti-Enabled (gift of D. Van Vactor) and mouse anti-α-tubulin (DM1A; Sigma) and detected with HRP anti-rabbit or anti-mouse (Jackson Labs, Bar Harbor, USA) with ECL Western Blotting Analysis System (Amersham Bioscience Corp., Piscataway, USA).

Alternatively, cells were lysed in 1 ml TRIzol (Invitrogen) and processed for total RNA resuspensions. Quantitated RNA samples (Bioanalyzer; Agilent Technologies, Palo Alto, USA) were normalized for reverse transcription reactions with SuperScript III (Invitrogen), then diluted cDNA was used for quantitative PCR (LightCycler FastStart DNA Master SYBR Green I, Roche Applied Science, Indianapolis, USA). Analyzed products were assayed in triplicates in multiple experiments. Individual samples were averaged, then normalized according to an adjustment factor, determined by the difference between cell types in the cross-point or cycle measurement for the *rp49*-positive control product. Relative levels of expression in the two cell types were presented as the difference between the averaged and adjusted cross-points (with one cycle difference approximately equivalent to a two-fold difference in expression level).

Additional data files

The following are provided as additional materials with this article online: the gene identity and primer sequences for dsRNAs used in the RNAi screens (Additional data file 1); the genes identified with phenotypes in the RNAi screens, organized by predicted functional class (Additional data file 2).

Acknowledgements

We thank S. Armknecht for technical help, members of the Institute for Chemistry and Cell Biology and the Mitchison laboratory (Harvard Medical School) for generous use of equipment and technical help, FlyBase for gene information, D. Traver and F. Schöck for helpful comments on the manuscript, and Howard Hughes Medical Institute (N.P. and B.B.), Jane Coffin Child's Memorial Fund (A.A.K.), and the UK Medical Research Council (A.C. and M.R.J.) for financial support.

References

1. Fraser AG, Kamath RS, Zipperlen P, Martinez-Campos M, Sohrmann M, Ahringer J: **Functional genomic analysis of *C. elegans* chromosome I by systematic RNA interference.** *Nature* 2000, **408:**325-330.
2. Gonczy P, Echeverri G, Oegema K, Coulson A, Jones SJ, Copley RR, Duperon J, Oegema J, Brehm M, Cassin E, *et al.*: **Functional genomic analysis of cell division in *C. elegans* using RNAi of genes on chromosome III.** *Nature* 2000, **408:**331-336.
3. Somma MP, Fasulo B, Cenci G, Cundari E, Gatti M: **Molecular dissection of cytokinesis by RNA interference in *Drosophila* cultured cells.** *Mol Biol Cell* 2002, **13:**2448-2460.
4. Adams MD, Celniker SE, Holt RA, Evans CA, Gocayne JD, Amanatides PG, Scherer SE, Li PW, Hoskins RA, Galle RF, *et al.*: **The genome sequence of *Drosophila melanogaster*.** *Science* 2000, **287:**2185-2195.
5. Rubin GM: **Biological annotation of the *Drosophila* genome sequence.** *Novartis Found Symp* 2000, **229:**79-83.
6. Clemens JC, Worby CA, Simonson-Leff N, Muda M, Maehama T, Hemmings BA, Dixon JE: **Use of double-stranded RNA interference in *Drosophila* cell lines to dissect signal transduction pathways.** *Proc Natl Acad Sci USA* 2000, **97:**6499-6503.
7. Echalier G, Ohanessian A: ***In vitro* culture of *Drosophila melanogaster* embryonic cells.** *In Vitro* 1970, **6:**162-172.
8. Schneider I: **Cell lines derived from late embryonic stages of *Drosophila melanogaster*.** *J Embryol Exp Morphol* 1972, **27:**353-365.
9. Yanagawa S, Lee JS, Ishimoto A: **Identification and characterization of a novel line of *Drosophila* Schneider S2 cells that respond to wingless signaling.** *J Biol Chem* 1998, **273:**32353-32359.

10. Prokopenko SN, Brumby A, O'Keefe L, Prior L, He Y, Saint R, Bellen HJ: **A putative exchange factor for Rho1 GTPase is required for initiation of cytokinesis in *Drosophila*.** *Genes Dev* 1999, **13:**2301-2314.
11. Hartwell LH, Culotti J, Reid B: **Genetic control of the cell-division cycle in yeast. I. Detection of mutants.** *Proc Natl Acad Sci USA* 1970, **66:**352-359.
12. **FlyBase** [http://flybase.bio.indiana.edu]
13. Hay BA, Wassarman DA, Rubin GM: ***Drosophila* homologs of baculovirus inhibitor of apoptosis proteins function to block cell death**. *Cell* 1995, **83:**1253-1262.
14. Wear MA, Schafer DA, Cooper JA: **Actin dynamics: assembly and disassembly of actin networks.** *Curr Biol* 2000, **10:**R891-R895.
15. Eichinger L, Bahler M, Dietz M, Eckerskorn C, Schleicher M: **Characterization and cloning of a *Dictyostelium* Ste20-like protein kinase that phosphorylates the actin-binding protein severin.** *J Biol Chem* 1998, **273:**12952-12959.
16. Drewes G, Ebneth A, Preuss U, Mandelkow EM, Mandelkow E: **MARK, a novel family of protein kinases that phosphorylate microtubule-associated proteins and trigger microtubule disruption**. *Cell* 1997, **89:**297-308.
17. Geiger B, Bershadsky A, Pankov R, Yamada KM: **Transmembrane crosstalk between the extracellular matrix-cytoskeleton crosstalk.** *Nat Rev Mol Cell Biol* 2001, **2:**793-805.
18. Graner MW, Bunch TA, Baumgartner S, Kerschen A, Brower DL: **Splice variants of the *Drosophila* PS2 integrins differentially interact with RGD-containing fragments of the extracellular proteins tiggrin, ten-m, and D-laminin 2.** *J Biol Chem* 1998, **273:**18235-18241.
19. Brown NH, Gregory SL, Rickoll WL, Fessler LI, Prout M, White RA, Fristrom JW: **Talin is essential for integrin function in *Drosophila*.** *Dev Cell* 2002, **3:**569-579.
20. Rogers SL, Rogers GC, Sharp DJ, Vale RD: ***Drosophila* EB1 is important for proper assembly, dynamics, and positioning of the mitotic spindle.** *J Cell Biol* 2002, **158:**873-884.
21. Madaule P, Eda M, Watanabe N, Fujisawa K, Matsuoka T, Bito H, Ishizaki T, Narumiya S: **Role of citron kinase as a target of the small GTPase Rho in cytokinesis.** *Nature* 1998, **394:**491-494.
22. Roy F, Laberge G, Douziech M, Ferland-McCollough D, Therrien M: **KSR is a scaffold required for activation of the ERK/MAPK module.** *Genes Dev* 2002, **16:**427-438.
23. Nusslein-Volhard C, Wieschaus E: **Mutations affecting segment number and polarity in *Drosophila*.** *Nature* 1980, **287:**795-801.
24. Simon MA, Bowtell DD, Dodson GS, Laverty TR, Rubin GM: **Ras1 and a putative guanine nucleotide exchange factor perform crucial steps in signaling by the sevenless protein tyrosine kinase.** *Cell* 1991, **67:**701-716.
25. Maehama T, Dixon JE: **The tumor suppressor, PTEN/MMAC1, dephosphorylates the lipid second messenger, phosphatidylinositol 3,4,5-trisphosphate.** *J Biol Chem* 1998, **273:**13375-13378.
26. Yamada KM, Araki M: **Tumor suppressor PTEN: modulator of cell signaling, growth, migration and apoptosis.** *J Cell Sci* 2001, **114:**2375-2382.
27. van Blitterswijk WJ, Houssa B: **Properties and functions of diacylglycerol kinases**. *Cell Signal* 2000, **12:**595-605.
28. Yang N, Higuchi O, Ohashi K, Nagata K, Wada A, Kangawa K, Nishida E, Mizuno K: **Cofilin phosphorylation by LIM-kinase 1 and its role in Rac-mediated actin reorganization.** *Nature* 1998, **393:**809-812.
29. **Berkeley *Drosophila* Genome Project** [http://www.fruitfly.org]
30 **NCBI BLAST** [http://www.ncbi.nlm.nih.gov/BLAST]
31. **Primer3** [http://www-genome.wi.mit.edu/genome_software/other/primer3.html]
32. Schuler GD: **Electronic PCR: bridging the gap between genome mapping and genome sequencing.** *Trends Biotechnol* 1998, **16:**456-459.
33. **Gene Ontology Consortium** [http://www.geneontology.org]